



HOKKAIDO UNIVERSITY

Title	Formation of Nanostructured Anodic Films on Iron and Their Electrode Applications [an abstract of entire text]
Author(s)	Fadillah, Laras
Description	この博士論文全文の閲覧方法については、以下のサイトをご参照ください。 https://www.lib.hokudai.ac.jp/dissertations/copy-guides/
Degree Grantor	北海道大学
Degree Name	博士(工学)
Dissertation Number	甲第14472号
Issue Date	2021-03-25
Doc URL	https://hdl.handle.net/2115/84299
Type	doctoral thesis
File Information	Laras_Fadillah_summary.pdf



学位論文の要約

博士の専攻分野の名称 博士（工学） 氏名 Laras Fadillah

学位論文題名

Formation of Nanostructured Anodic Films on Iron and Their Electrode Applications (鉄へのナノ構造アノード酸化皮膜の形成と電極応用)

Anodizing of valve metals such as Ti, Nb, Ta, W and Al has become a subject of scientific interest in recent years in view of possibilities to form self-organized nanoporous and nanotubular anodic films on metal substrate. An extension of anodizing process to iron group metals opens the way for applications of nanostructured oxides in cost-effective electrochemical devices such as those used in energy conversion and storage systems. The current thesis focuses on anodizing of Fe and electrochemistry of self-organized nanotubes/nanopores in order to estimate the possibility of application in energy storage devices. Anodic iron oxide has not been extensively explored so far in electrochemical devices, among which hematite (Fe_2O_3) is a promising photoanode for water splitting and negative electrode material for lithium-ion batteries. The objective of the present study is the fundamental understanding of the growth of anodic nanopores/nanotubes on iron implicating the studies on iron single crystals for evaluation on how the anodic film grows depending on facet index number. The modification of the anodic film growth by the addition of an alloying element is studied to the control full transition between nanopores and nanotubes in order to meet the requirements of high surface area for desired applications and physicochemical parameters such as bandgap engineering. Further, the functionality of nanostructured anodic iron oxide films for photocatalytic water splitting and lithium-ion battery applications is investigated. This dissertation includes seven chapters, and the organization is explained below.

The background of this study including the details of anodizing process and specific objectives of this dissertation are described in Chapter 1. Chapter 2 consists of theoretical and practical details of the techniques used in the present study.

Chapter 3 describes the investigations of the effect of the crystallographic orientation of iron on the anodizing process. Anodizing of Fe (100), Fe (100), and Fe (100) single crystals in ethylene glycol electrolyte containing 1.5 mol dm^{-3} water and 0.1 mol dm^{-3} ammonium fluoride leads to the formation of anodic nanopores/nanotubes where the nanopores are essentially composed of oxide

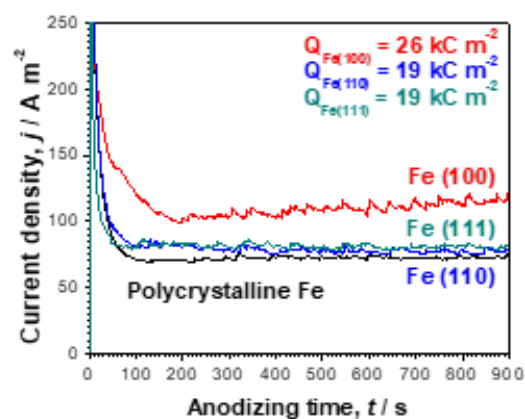


Figure 1. Current-time (j - t) responses for polycrystalline, (100), (110) and (111).

nanotubes separated by iron fluoride cell boundaries. Figure 1 shows the current-time (j-t) transients of Fe (100), Fe (100), and Fe (100) at 20°C temperature at 60 V anodizing. Significant differences in the current density values were found on j-t curves depending on single-crystal indexing number. The current density in the steady-state growth on Fe (100) is larger than that on Fe (110) and Fe (111) by a factor of 1.4; the author assumes that both the ionic current and electronic current may be involved in the anodizing process.

The morphology of nanoporous film formation is apparently independent of the index number of facets on which the anodic film is formed (Figure 2.). The uniform morphology of anodic iron oxide was observed on all of the grain orientation, nanoporous with the $2.2 \pm 0.1 \mu\text{m}$, $2.1 \pm 0.1 \mu\text{m}$, and $2.1 \pm 0.1 \mu\text{m}$ thickness for (100), (111) and (110), respectively and the other structural parameters, such as the pore diameter, interpore distance, barrier thickness are not significantly affected.

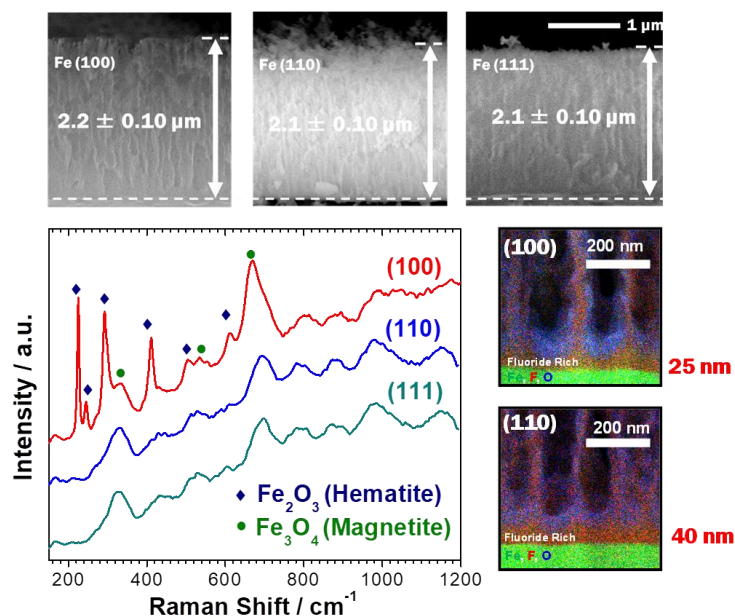


Figure 2. Raman spectra of anodic porous film grown on Fe (100), Fe (110) & Fe (111), and HR-EDS of nanoporous film on Fe (100) & Fe (110).

Nevertheless, the EDS compositional maps (Figure 2.) show anisotropic dependencies to the growth formation of iron oxides. Two layers were found on anodic films on Iron; FeF_2 (fluoride-rich layer) and the iron oxides (oxide-rich layer). Thinner fluoride-rich layer on anodic films on Fe (100) compared to Fe (110) might cause higher electric current due to insulative nature of FeF_2 . The differences also observed on Raman spectroscopy, the anodic films formed on Fe (110) and Fe (111) are essentially amorphous and exhibits typical magnetite (Fe_3O_4), whereas the one formed on Fe (100) facet shows high degree of crystallinity and the spectral signatures characteristic for hematite (Fe_2O_3). The crystallization upon anodic film growth also one of the possible reasons for modification of electronic properties followed by extensive oxygen evolution on hematite (Fe_2O_3) nanocrystals observed on (100) facet. The variations in the growth may be possible if one considers following physicochemical properties of iron: i) planar atomic density and corresponding ii) compressive stress.

In Chapter 4, the effect of alloying of sputter-deposited Fe with 9 at.% tungsten on the growth of nanoporous anodic oxide was studied in ethylene glycol electrolyte containing 0.1 mol dm^{-3} ammonium fluoride and 1.5 mol dm^{-3} water. In the present study, anodizing behavior of Fe-W alloy was studied and compared with that of iron for a better understanding the growth mechanism of the anodic films on iron and iron-base alloys in fluoride-containing organic electrolytes. The classic nanoporous anodic film (Al_2O_3 -like) is developed on pure Fe while the transition of nanopores to nanotubes (TiO_2 -like) is observed for anodizing of Fe-W alloy (Figure 2). The pores/nanotubes having average diameter 50-110 nm and 30-60 nm are formed on pure Fe and Fe-W alloy at voltage

40-60 V, respectively. Both nanoporous/nanotubular anodic films grow in line with the field-assisted flow model with a few fundamental details: i) transition of nanopores to nanotubes occurs upon anodizing of Fe-W alloy, ii) significant reduction of the cell size (nanotube diameter) is obtained on Fe-W alloy.

The shape of nanotubes is evident from high angle annular dark field (HAADF) images of a FIB lamella for Fe-W alloy anodized at 60 V (Figure 4). The regions with a lighter appearance on TEM micrograph correspond to nanotube walls composed of mixed tungsten/iron oxide containing fluorides. A relatively thick layer at the alloy/oxide interface is produced at Fe-W alloy/oxide interface, and its thickness varies across the FIB lamella. Such large thickness variations cannot be caused by an electrochemical reaction as the high electric field is primarily localized in the barrier-layer forming uniform anodic layer depending on the applied voltage, possible reason of this layer is from chemical reaction due to exposition of structure to moisture. ToF-SIMS mass spectra detect WF_6 domains and their decomposed forms in the nanotubular film. Taking into account fast inward-migration of F^- and very slow outward-migration of W^{6+} species in anodic film, the primary location of WF_6 compound should be the bottom of barrier-layer which is switched to the cell boundary position due to stress generated at the barrier-layer and material flow according to the field-assisted flow model. The transition of nanoporous to nanotubes as well as chemical changes is discussed in view of effective modification of the cell boundary region with WF_6 compound upon the growth of anodic film under the influence of high electric field strength (Figure 4). A possible reason for developing the space between nanotubes is the faster kinetics of WF_6 reaction with water. Alloying of iron is an effective way to modify the anodic film's nanostructure on iron. The thick layer formed at the FeW-alloy/oxide interface is possibly a result of chemical reaction of WF_6 with alloy at anodic film base due to the exposition of structure to moisture.

The photocatalytic properties of anodized Fe-W alloy were explored in Chapter 5. Two types of anodic films were developed on the Fe-W alloy: a barrier-type, using 0.1 M of water in ethylene-glycol electrolyte for 30 s, and a nanotubular-type, using 1.5 mol dm^{-3} water in ethylene-glycol electrolyte for 150 s. Their photocatalytic properties were compared with those of the nanoporous-type anodic film formed on iron. They were annealed at high temperatures to get sufficiently crystallized oxides and to remove fluorine species. The photocurrent of the Fe-W alloy specimens

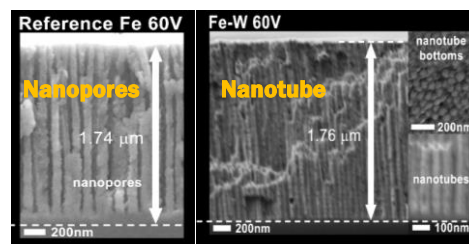


Figure 3. Cross-section SEM images of nanopores/nanotubes formed by anodizing of Fe-W alloy at 60 V.

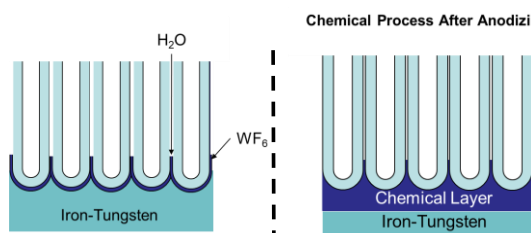
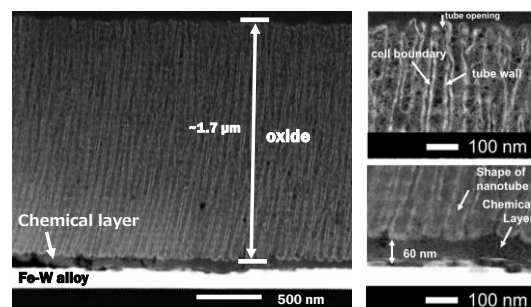


Figure 4. HAADF images of anodic film on Fe-W alloy and schematic illustrations of proposed growth mechanism for nanopores/nanotubes formed on Fe and Fe-W alloy.

with the nanotubular and barrier oxide films is remarkably higher than that of the iron with the nanoporous layer. In addition, enhanced photodegradation of methylene blue under the presence of the anodized Fe-W alloy specimens is found in comparison with that under the anodized iron. The concentration changes C/C_0 versus time for photo-degradation of methylene blue on the anodic nanopores iron oxide exhibited a limited photocatalytic performance towards degradation with an efficiency of 9.2% after 180-min irradiation. On the other hand, the high adsorption capacity of the Fe-W sample can be inferred from a large amount of dye removal (40-60 %) under exposure to visible light irradiation. The enhancement in photocatalytic performance of the Fe_2O_3 containing tungsten can be attributed to the improved absorption ability and efficient electron-hole transfer at the interfaces of anodic films.

The nanotubular-type specimen shows high photocurrent and photodegradation properties. STEM and HR-TEM showed the dispersion of Fe_2WO_6 nanoparticles on the anodic film grown on Fe-W Alloy. It is likely that $\text{Fe}_2\text{O}_3(\text{Fe}_3\text{O}_4)/\text{Fe}_2\text{WO}_6$ hybrids were developed because the solubility of tungsten species into iron oxides is very limited at thermodynamic equilibrium. The development of such hybrids may effectively separate the photogenerated electron-hole pairs at the heterojunction, resulting in high photocatalytic properties. Hence, the nanotubular-type of Fe-W oxide is a possible candidate for visible-light-driven photocatalysts.

The performance of anodic nanoporous/nanotubular films grown on iron for lithium-ion battery application is examined (Chapter 6). The iron oxide nanotubes formed by anodizing of polycrystalline iron in ethylene glycol electrolyte containing 0.1 mol dm^{-3} ammonium fluoride and 1.5 mol dm^{-3} water were thermally treated at 350-500 °C in order to control the crystallographic structure of the oxide. An increase of crystallinity, the increased ratio of hematite (Fe_2O_3) to magnetite (Fe_3O_4) and elimination of the fluorides are observed with an increase in annealing temperature. Galvanostatic cycling with potential limitation (GCPL) was carried out to investigate in detail the electrochemical activity of nanotubular/nanoporous anodic film in the lithiation process. The succeeding anodic scan shows the broad anodic $dQ.dE^{-1}$ peak corresponding to oxidation of Fe^0 to Fe_2O_3 and Fe_3O_4 . The *in-situ* Raman spectroscopy and charge and discharge curves for the anodic films annealed at 500 °C reveal a quasi-reversible lithiation/delithiation process through Li_2O formation. The anodic films annealed at 500 °C exhibit relatively high areal capacity of 3.5 mA h cm^{-2} at a charge/discharge current density of $20 \mu\text{A cm}^{-2}$ assembled in the half-cell of lithium-ion battery. The cycling stability tests supported with optical microscopy observations of the negative electrode assembled in an electrochemical cell for *in-situ* measurements indicate adhesion problems, leading to a gradual decrease of rate capability mainly caused by the detachment of oxide.

Finally, the main findings of this dissertation are summarized, and future prospects are given in Chapter 7.